

Soft Matter

Accepted Manuscript



This is an *Accepted Manuscript*, which has been through the Royal Society of Chemistry peer review process and has been accepted for publication.

Accepted Manuscripts are published online shortly after acceptance, before technical editing, formatting and proof reading. Using this free service, authors can make their results available to the community, in citable form, before we publish the edited article. We will replace this *Accepted Manuscript* with the edited and formatted *Advance Article* as soon as it is available.

You can find more information about *Accepted Manuscripts* in the [Information for Authors](#).

Please note that technical editing may introduce minor changes to the text and/or graphics, which may alter content. The journal's standard [Terms & Conditions](#) and the [Ethical guidelines](#) still apply. In no event shall the Royal Society of Chemistry be held responsible for any errors or omissions in this *Accepted Manuscript* or any consequences arising from the use of any information it contains.

Buckling of an elastic fiber with finite length in a soft matrix†

Yan Zhao, Jing Li, Yan Ping Cao*, Xi-Qiao Feng

Institute of Biomechanics and Medical Engineering, AML, Department of Engineering Mechanics,

Tsinghua University, Beijing 100084, P. R. China

† Electronic supplementary information (ESI) available.

Abstract: Elastic fibers embedded in a soft matrix are frequently encountered in nature and engineering across different length scales, ranging from microtubules in cytosol and filament networks to dissociative slender fish bones in muscles and fiber-reinforced soft composites. The fibers may buckle when the composite is subjected to compression; this study investigates this issue through a combination of experiments, finite-element simulations and theoretical analysis. The analysis reveals the important role of the interfacial shear forces and leads to an explicit solution to predict the occurrence of buckling for a slender fiber with finite length. The results reported in this paper will help understand the formation of shapes in some natural systems and provide guidelines for the design of soft biocomposites.

*Corresponding author: caoyanping@tsinghua.edu.cn (Y. P. Cao)

1. Introduction

Elastic fibers embedded in a soft substrate are ubiquitous in nature and engineering, such as microtubules in living cells (Fig. 1a),¹⁻⁶ amyloid fibrils (Fig. 1b),⁷⁻⁹ electrodes implanted in biological tissues (Fig. 1c),¹⁰ growing plant roots in soil,^{11, 12} dissociative fish bones in fish muscle, and fiber-reinforced polymer composites (Fig. 1d).¹³ When subjected to compressive loads, isolated fibers may exhibit classical Euler buckling. However, fibers embedded in a soft matrix may buckle in a mode with a considerably shorter wavelength and can sustain considerably higher compressive loads than that of Euler buckling.^{6, 14-16} Microtubule buckling has drawn considerable attention in recent years^{6, 14, 17-20} due to its importance in cell biology. Buckling of stiff fibers in a soft matrix is also of interest in many other biological and engineering systems. For example, the amyloid fibrils (Fig. 1b) associated with several major diseases, including Alzheimer's, Parkinson's and Creutzfeldt-Jakob disease,²¹ are stiff fibers surrounded by a soft matrix⁹ that may buckle due to differential growth. Electrodes (Fig. 1c) are widely used for deep brain stimulations¹⁰ and can be regarded as stiff fibers with finite length embedded in soft tissues. Buckling should be avoided when this process is successful. Plant roots, which play a key role in plant growth and crop productivity,¹¹ may buckle in soil during growth. Most previous works on the buckling of an elastic fiber in a soft matrix focused on the case in which the fiber length was infinite and/or the compressive load was directly imposed on its two ends.^{14, 18, 19, 22, 23} However, in many practical composite systems, the fibers have finite length and the compression is

applied to the matrix rather than directly imposed on the two ends of a fiber. The fibers sense the compressive strain mainly through the interfacial tractions, and in this case, the critical conditions for the onset of buckling remain elusive due to the challenges in determining the interfacial tractions. This issue is addressed in this study through a combination of experiments, finite element simulations and theoretical analysis.

The remainder of this paper is organized as follows. Experiments are discussed in Section 2 to investigate the buckling of an elastic fiber with finite length in a soft matrix. In particular, the buckling of hairs with different lengths embedded in a soft PDMS substrate was investigated and revealed that the critical compressive strain imposed on the substrate for buckling onset depended strongly on the fiber length. A theoretical analysis is presented in Section 3 to quantitatively understand the experiments. The analysis revealed the important role played by the interfacial shear traction and leads to an analytical solution for the critical compressive strain in the substrate for buckling onset. Section 4 discusses the potential applications of the method and results. Section 5 offers the concluding remarks.

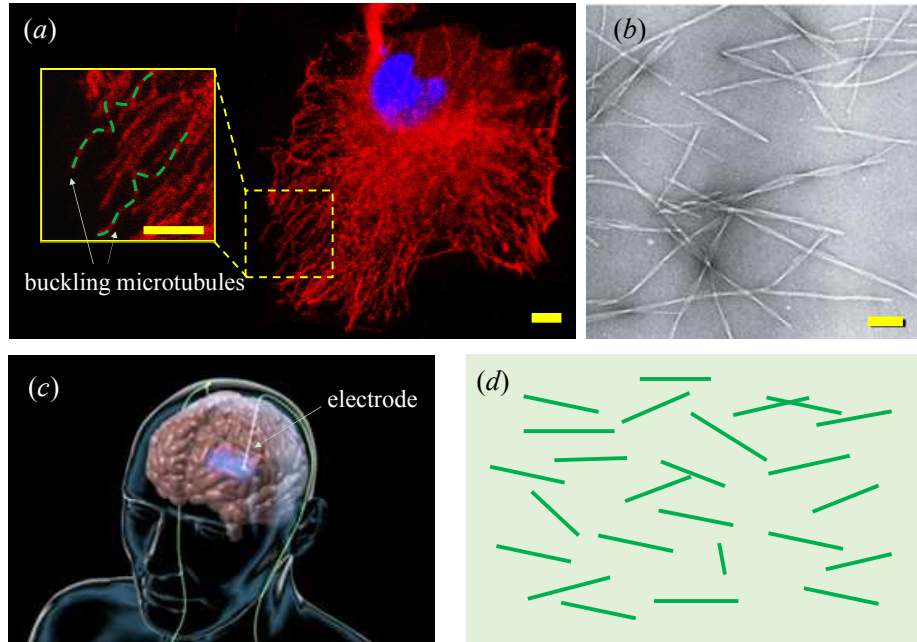


Fig. 1. Several examples of fibers in a soft substrate encountered in nature and engineering: (a) buckling of microtubules in living cells, scale bar: 5 μm . Experimental details on the observation of buckled microtubules are given in Supplementary Information (S1); (b) amyloid fibrils,⁹ scale bar: 100 nm; (c) electrode implanted in brain; (d) fiber-reinforced composites.

2. Experiments

Human hairs with radius of approximately 50 μm were chosen as elastic fibers, and the soft substrate was made of poly(dimethylsiloxane) (PDMS). The PDMS bulk was prepared by mixing the base and crosslinker (Sylgard 184, Dow Corning) at a ratio of 40:1 w/w. First, half of the pre-mixture was filled in a rectangular box and cured at 60°C for 12 h after it was degassed in a vacuum pump. Then, straight hairs with different lengths, i.e., 0.5, 1, 2, and 3 cm, were attached on the surface of the cured PDMS. Finally, the remainder of the mixture was filled into the rectangular box and cured at 60°C for another 12 h. Then, the sample with the size of 30×38×45

mm was prepared (Fig. 2a). The slenderness ratios c of the hairs (i.e., the length-radius ratios) were 100, 200, 400, and 600 for the 0.5-, 1-, 2-, and 3-cm-long hairs, respectively. $c \gg 1$ in these experiments, ensuring that the hairs were slender fibers. Indentation tests were performed to measure the shear modulus of the soft PDMS (40:1 w/w), which was approximately 0.043 MPa. The elastic modulus of the hair given by the tensile tests was approximately 5.6 GPa. Both indentation tests and tensile tests were conducted using the Bose ElectroForce3100® test instrument.

An isolated hair would undergo Euler buckling when it was compressed. Unlike the buckling behavior of an isolated hair, a long hair embedded in the soft PDMS would exhibit a short-wavelength buckling mode (Fig. 2). Interestingly, buckling was always first observed in the central region of the hair. Furthermore, these experiments showed that the hair slenderness ratio significantly affected the buckling behavior of the system. When the PDMS was compressed, the longest hair (3 cm) buckled at a small compression amount of approximately 2%, and the buckling amplitude increased with increases in the externally compressive strain. Afterward, the 2-cm-long hair buckled when the overall compressive (nominal) strain was approximately 7% (Fig. 2c). Buckling clearly occurred in the 1-cm-long hair only when the compressive strain reached approximately 17%. The shortest hair (0.5 cm) maintained a straight configuration and did not buckle during the entire compression process. The critical compressive strain of the hair with infinite length (i.e., the length of the fiber is considerably greater than the wrinkling wavelength) embedded in soft PDMS (1:40) was approximately 0.3% according to the theoretical solution in Section

3, which was extremely small. These experimental results clearly show that the critical compressive strain for the buckling of fibers strongly depends on their lengths and can be increased by several orders of magnitude by tuning the slenderness ratio of the fiber.

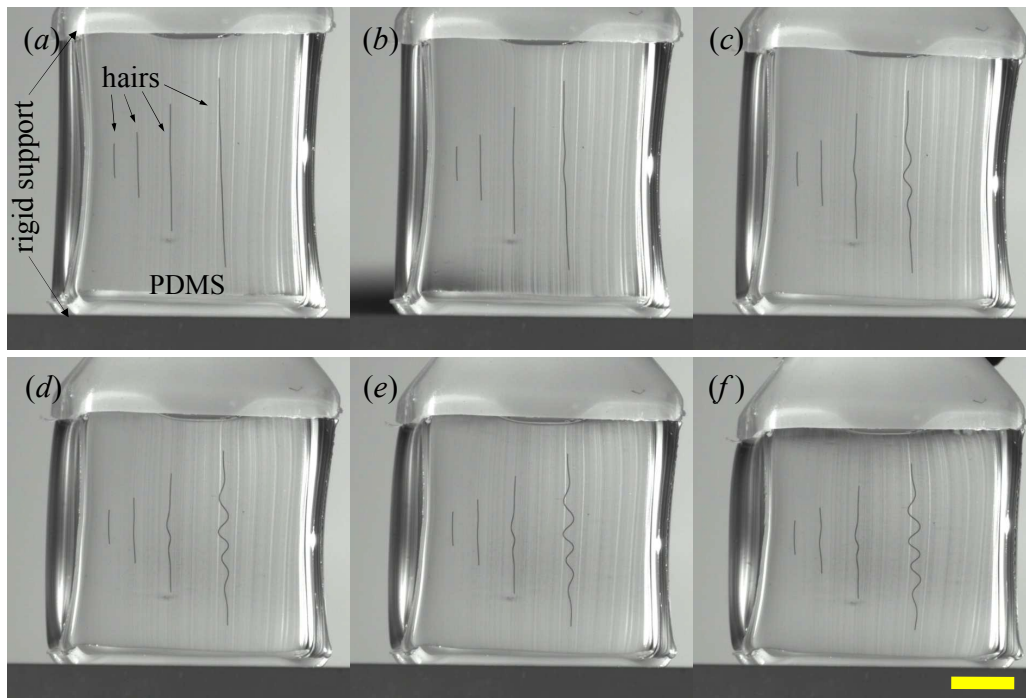


Fig. 2. Sequence of buckling patterns of hairs with finite lengths embedded in a soft substrate. The overall compressive strain imposed on the substrate was (a) 0%; (b) 2%; (c) 7%; (d) 12%; (e) 13%; (f) 17%. Scale bar: 1 cm.

3. Theoretical analysis

Next, a theoretical analysis is performed to understand the buckling mechanisms behind the experiments in Section 2 and, in particular, the dependence of the critical compressive strain on the mechanical and geometrical parameters of the system. An elastic and stiff fiber embedded in an elastic medium was considered, as shown in Fig.

3. E and ν refer to the elastic modulus and Poisson's ratio, respectively, and the subscripts "f" and "s" refer to the fiber and substrate, respectively. The substrate is subjected to axial compression along the z direction, with the overall compressive strain ε_0 . The coordinate system is shown in Fig. 3. The fiber is assumed to be a long cylinder of length $2a$ and radius r . The interface between the fiber and substrate is perfectly bonded. The fiber buckled when ε_0 reached a critical value.

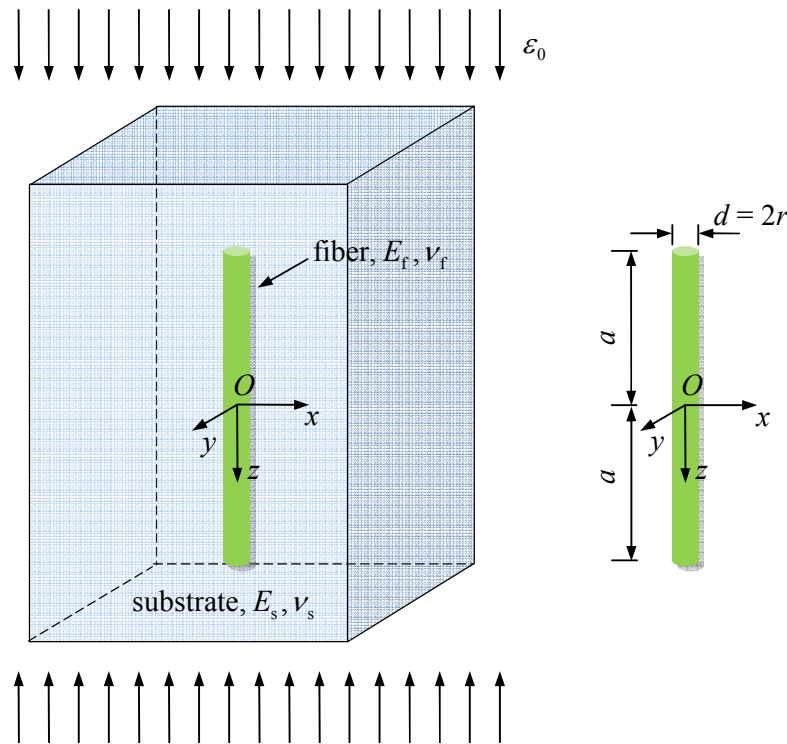


Fig. 3 Theoretical model of an elastic fiber embedded in soft substrate subjected to compression.

3.1 Interfacial tractions

In the considered problem, the fiber buckled due to the interfacial tractions. In the 1950s, a shear-lag model was proposed to estimate the stress transfer between the

fiber and soft matrix in fiber-reinforced composites.²⁴ However, analytical determination of the interfacial tractions is a challenging issue.^{25, 26} Furthermore, Nairn showed that the shear-lag model is not applicable to the case of a fiber embedded in an infinite matrix (or low volume fractions of fibers).²⁷ Inspired by recent studies on the buckling of a stiff film resting on a soft substrate,^{28, 29} finite element (FE) simulations using the general purpose software ABAQUS were conducted to investigate the interfacial tractions. The model contained more than 50,000 axisymmetric quadratic elements (CAX8R). Uniaxial compression was imposed on the substrate. Both the fiber and substrate were assumed to be weakly compressible, with Poisson's ratios of $\nu_s = \nu_f = 0.48$. Based on the FE results shown in Fig. 4, the interfacial shear traction T_z between the fiber and substrate was assumed to be

$$T_z = \begin{cases} A \ln \frac{a+z}{a} + B \frac{z}{a}, & -a < z \leq 0 \\ -A \ln \frac{a-z}{a} + B \frac{z}{a}, & 0 \leq z < a \end{cases}, \quad (1)$$

where the parameters A and B were determined from the two compatibility conditions given below. Eq. (1) was chosen to fit the FE results, and other functions may be applicable, provided they can match the FE results well.

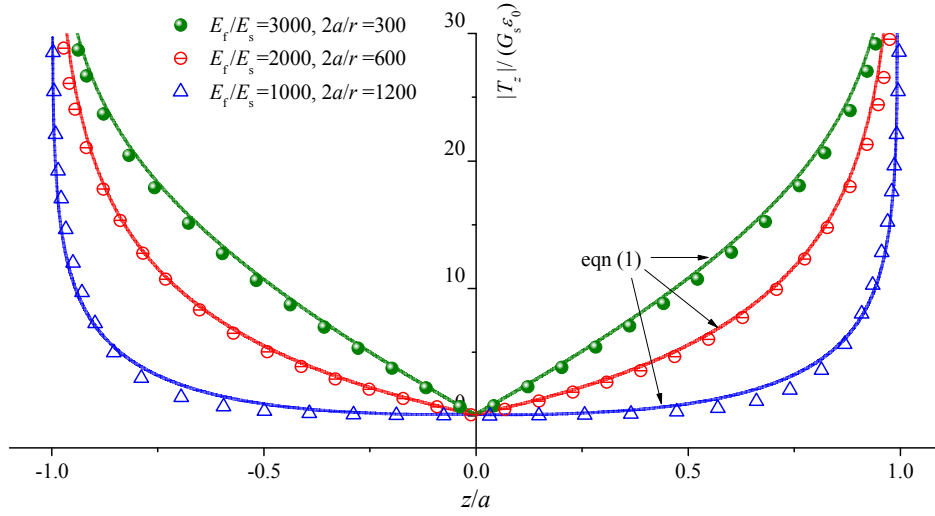


Fig. 4 Distribution of the interfacial traction. The points are FE results, and the lines are the predicted results by eqn (1).

3.2 Relation between the fiber strain and overall strain in the substrate

The compatibility conditions require that the normal strains in the fiber along the z direction are the same as those in the substrate at points $(x=0, y=0, z=0)$ and $(x=0, y=0, z=a/2)$, i.e.,

$$\begin{aligned} \epsilon_z^f \Big|_{z=0} &= \epsilon_z^s \Big|_{x=0, y=0, z=0} \\ \epsilon_z^f \Big|_{z=a/2} &= \epsilon_z^s \Big|_{x=0, y=0, z=a/2} \end{aligned} \quad (2)$$

The normal strain ϵ_z^f in the fiber under the load $-T_z$ can be determined by integrating the equilibrium equation:

$$\epsilon_z^f = -\frac{2}{E_f r} \int_z^a T_z dz = \frac{2A}{E_f r} \left[(a-z) \ln \frac{a-z}{a} - (a-z) \right] - \frac{B}{E_f a r} (a^2 - z^2). \quad 0 \leq z < a. \quad (3)$$

Eq. (3) clearly shows that the compressive strain in the fiber is not uniform and that the maximum compressive strain occurs when $z \rightarrow 0$, which is given by

$$\epsilon = -\epsilon_z^f \Big|_{z=0} = \frac{2A+B}{E_f} \frac{a}{r}. \quad (4)$$

This may explain the buckling phenomenon of the hair (Fig. 2), i.e., buckling first occurs in the central region. From eqn (3), the normal strain at the point $(x = 0, y = 0, z = a/2)$ of the fiber is determined as

$$\varepsilon_z^f \Big|_{z=a/2} = -\frac{1}{E_f} \frac{a}{r} \left[A(1 + \ln 2) + \frac{3}{4} B \right]. \quad (5)$$

The strain state in the substrate under the interfacial tractions given by eqn (1) can be obtained using Kelvin's solution. For an infinite elastic medium under a unit force at point $(\sqrt{x^2 + y^2} = r, z)$, the strain component ε_z^{s0} at point O is given by

$$\varepsilon_z^{s0} = \frac{1}{16\pi G_s(1-\nu_s^2)} \left[\frac{1-4\nu_s^2}{(r^2+z^2)^{3/2}} z + \frac{3z^3}{(r^2+z^2)^{5/2}} - \frac{3\nu_s z r^2}{(r^2+z^2)^{5/2}} \right], \quad (6)$$

where $G_s = \frac{E_s}{2(1+\nu_s)}$ is the shear modulus of the substrate. The strain at point O

induced by the interfacial force T_z can be obtained as

$$\begin{aligned} \varepsilon_z^{sT} \Big|_{x=0, y=0, z=0} &= -2\pi r \int_{-a}^a \varepsilon_z^{s0} \times T_z \, dz \\ &= -\frac{r}{4G_s(1-\nu_s^2)} \int_0^a \left[A \ln\left(1 - \frac{z}{a}\right) - B \frac{z}{a} \right] \times \left[\frac{1-4\nu_s^2}{(r^2+z^2)^{3/2}} z + \frac{3z^3}{(r^2+z^2)^{5/2}} - \frac{3\nu_s z r^2}{(r^2+z^2)^{5/2}} \right] dz \end{aligned} \quad (7)$$

The following analytical solution can be obtained from eqn (7):

$$\begin{aligned} \varepsilon_z^{sT} \Big|_{x=0, y=0, z=0} &= \frac{A}{2G_s(1-\nu_s^2)c} \frac{3-4\nu_s^2}{(1+4/c^2)^{1/2}} \ln \frac{1+4/c^2}{(2/c + \sqrt{1+4/c^2})/c} \\ &+ \frac{A}{2G_s(1-\nu_s^2)c} \left[\frac{4/c^2}{(1+4/c^2)^{3/2}} - \frac{2/c}{1+4/c^2} - \frac{1}{(1+4/c^2)^{3/2}} + \frac{1}{(1+4/c^2)^{3/2}} \ln \frac{1+4/c^2}{(2/c + \sqrt{1+4/c^2})/c} \right], \quad (8) \\ &- \frac{A\nu_s}{2G_s(1-\nu_s^2)c} \left[-\frac{4/c^2}{(1+4/c^2)^{3/2}} + \frac{2/c}{1+4/c^2} + \frac{1}{(1+4/c^2)^{3/2}} + \frac{4/c^2}{(1+4/c^2)^{3/2}} \ln \frac{1+4/c^2}{(2/c + \sqrt{1+4/c^2})/c} \right] \\ &+ \frac{2B}{G_s c} \left[\operatorname{arcsinh}\left(\frac{c}{2}\right) - \frac{1}{\sqrt{1+4/c^2}} \right] - \frac{B}{2G_s(1-\nu_s)c} \end{aligned}$$

where $c = 2a/r$ is the slenderness ratio of the fiber, which is a large number for a long fiber, i.e., $c \gg 1$ or $1/c \ll 1$. By neglecting the higher-order terms of $1/c$, eqn (8) can be simplified as

$$\varepsilon_z^{sT} \Big|_{x=0,y=0,z=0} = \frac{A+B}{G_s} \frac{2}{c} \ln c - \frac{A+B}{2G_s(1-\nu_s)c} - \frac{2B}{G_sc}. \quad (9)$$

Then, the overall strain in the z direction at point O is

$$\varepsilon_z^s \Big|_{x=0,y=0,z=0} = -\varepsilon_0 + \varepsilon_z^{sT} \Big|_{x=0,y=0,z=0}. \quad (10)$$

The normal strain at the upper end of the fiber ($x=0, y=0, z=a/2$) induced by $-T_z$ can be calculated by

$$\begin{aligned} \varepsilon_z^{sT} \Big|_{x=0,y=0,z=a/2} &= \frac{c}{4G_s(1-\nu_s^2)} \int_{-1/2}^{1/2} \left[-A \ln\left(\frac{1}{2}-t\right) + B\left(\frac{1}{2}+t\right) \right] \times \left[\frac{1-4\nu_s^2}{(c^2+t^2)^{3/2}} t + \frac{3t^3}{(c^2+t^2)^{5/2}} - \frac{3\nu_s c^2 t}{(c^2+t^2)^{5/2}} \right] dt \\ &+ \frac{c}{4G_s(1-\nu_s^2)} \int_{-1/2}^{-3/2} \left[A \ln\left(\frac{3}{2}+t\right) + B\left(\frac{1}{2}+t\right) \right] \times \left[\frac{1-4\nu_s^2}{(c^2+t^2)^{3/2}} t + \frac{3t^3}{(c^2+t^2)^{5/2}} - \frac{3\nu_s c^2 t}{(c^2+t^2)^{5/2}} \right] dt \end{aligned} \quad (11)$$

Its solution is

$$\varepsilon_z^{sT} \Big|_{x=0,y=0,z=a/2} = \frac{2A}{G_sc} \left[-\ln(16/c^2) + \frac{1}{3} \ln 3 - 2 + \frac{3-4\nu_s}{2(1-\nu_s)} \right] + \frac{2B}{G_sc} \left[\ln \frac{\sqrt{3}}{2} c - \frac{4}{3} - \frac{1}{4(1-\nu_s)} \right]. \quad (12)$$

The higher-order terms of $1/c$ in eqn (12) was neglected. The overall strain along the z axis at the point of ($x=0, y=0, z=a/2$) is given by

$$\varepsilon_z^s \Big|_{x=0,y=0,z=a/2} = -\varepsilon_0 + \varepsilon_z^{sT} \Big|_{x=0,y=0,z=a/2}. \quad (13)$$

From the two compatibility conditions given by eqn (2), the coefficients A and B are determined as

$$A = \frac{h_1}{1+h_1} \frac{2}{c} E_f \varepsilon, \quad B = \frac{1-h_1}{1+h_1} \frac{2}{c} E_f \varepsilon, \quad (14)$$

where

$$h_1 = \frac{-\ln \frac{\sqrt{3}}{2} + \frac{1}{3} + \frac{1}{16} \frac{G_sc^2}{E_f}}{-\ln(8\sqrt{3}/c) + \frac{1}{3} \ln 3 - \frac{5}{3} + \frac{7-8\nu_s}{4(1-\nu_s)} + \left(\ln 2 - \frac{3}{4} \right) \frac{G_sc^2}{4E_f}}. \quad (15)$$

Figure 4 shows that the interfacial force given by eqns. (1) and (14) matches the FE results well.

Furthermore, the relation between ε_0 and ε can be obtained as

$$\varepsilon_0 = \varepsilon + \frac{h-1+h_1}{1+h_1} \frac{4E_f}{G_s c^2} \varepsilon, \quad (16)$$

where

$$h = \ln c - \frac{1}{4(1-\nu_s)}. \quad (17)$$

The maximum compressive strain in the fiber and the overall compressive strain in the substrate are shown in Fig. 5. The theoretical solution given by eqn (16) matches the FE results well. When the fiber length is infinite, i.e., $c \rightarrow \infty$, the maximum strain in the fiber is equal to ε_0 according to eqn (16). However, for a fiber with finite length, the compressive strain in the fiber is always smaller than the overall compressive strain in the substrate. Furthermore, for a large modular ratio E_f/E_s and small slenderness ratio $2a/r$, the fiber strain can be several orders of magnitude smaller than ε_0 (Fig. 5). This suggests that the strain state in the substrate can be tuned by controlling the fiber slenderness ratio. In the theoretical model, the substrate is assumed to be infinite, i.e., its axial length is considerably greater than the fiber length. However, in practical systems, the matrix has finite dimension. Therefore, the extent to which this assumption is valid was examined using FE simulations. The results are shown in Fig. 6, demonstrating that eqn (16) can provide a reasonable prediction of the maximum strain in the fiber even for the case when the axial length of the substrate is comparable to the fiber length ($L_s/2a$). For instance, the error is below 3% when $L_s/2a=1.5$ and is approximately 10% when $L_s/2a=1.1$.

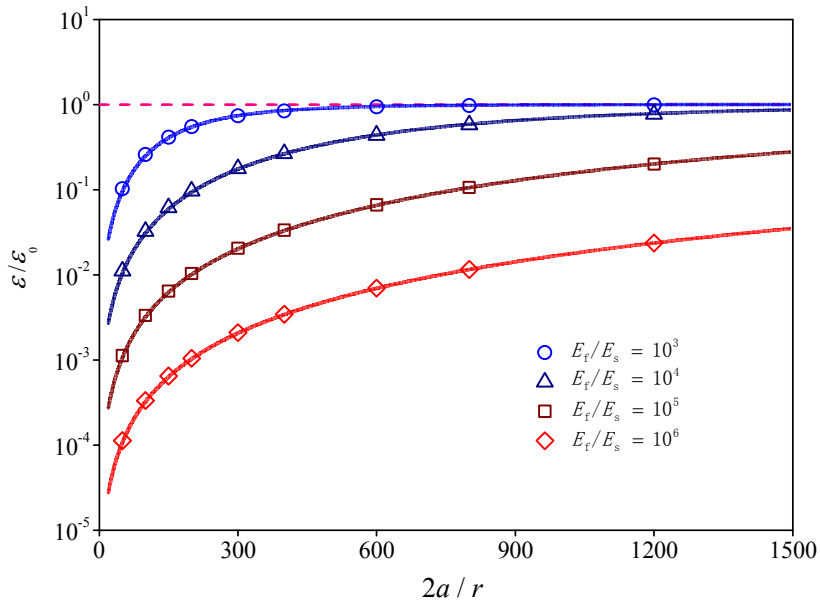


Fig. 5. Ratio of the maximum compressive strain in the fiber (ε) to the overall compressive strain in the substrate (ε_0). The lines are the theoretical solutions given by eqn (16), and the data points represent the FE results.

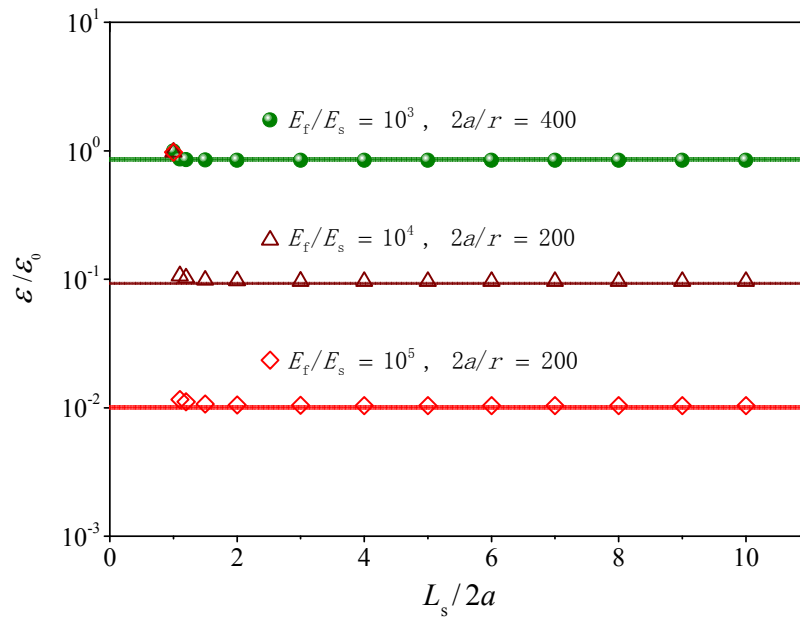


Fig. 6. Effect of substrate dimension on the maximum compressive strain in the fiber. L_s refers to the axial length of the matrix. The data points represent the FE results, and the corresponding lines are theoretical predictions.

3.3 Critical compressive strain in the substrate for the onset of buckling

Next, a fiber with infinite length, i.e., $1/c = 0$, is considered to analytically predict the buckling of an elastic fiber with finite length in a soft matrix. In this case, eqns (3), (14) and (16) indicate that the strain in the fiber is uniform and equals the overall compressive strain in the substrate, i.e.,

$$\varepsilon_z^f = \varepsilon = \varepsilon_0. \quad (18)$$

Considering the fiber as a slender beam, the equilibrium equation is

$$E_f I \frac{\partial^4 w}{\partial z^4} + E_f S \varepsilon_0 \frac{\partial^2 w}{\partial z^2} + K w = 0 \quad (19)$$

where $E_f I$ is the bending stiffness of the fiber and S is the cross-sectional area. $w = A \cos kz$ is the buckling mode with A and $k = 2\pi/\lambda$ as the amplitude and wavenumber, respectively. λ is the buckling wavelength. K is the effective stiffness of the soft foundation, and its explicit expression is obtained through the integration of Kelvin's solution (Supporting Information, S2)

$$K = \frac{4\pi G_s^*}{-\ln(2kr/5)}, \quad (20)$$

where $G_s^* = \frac{2(1-\nu_s)}{3-4\nu_s} G_s$. For an incompressible material, i.e., $G_s^* = G_s$, eqn (20) is consistent with the foundation stiffness obtained from the strain energy of the substrate given by Jiang and Zhang.¹⁸ Eqn (20) is also consistent with the foundation stiffness adopted in Brangwynne *et al.*¹⁴ and Su *et al.*²³ when $kr \rightarrow 0$.

Eq. (19) yields

$$E_f S \varepsilon = E_f I k^2 + \frac{K}{k^2}. \quad (21)$$

Minimizing eqn (21) with respect to the wavenumber k gives the critical buckling strain as

$$E_f S \varepsilon^c = E_f I k_c^2 + \frac{4\pi G_s^*}{-k_c^2 \ln(2k_c r/5)}, \quad (22)$$

where k_c is the critical buckling wavenumber and is determined by the following equation:

$$k_c = \left(\frac{2\pi G_s^*}{E_f I} \right)^{1/4} \left[\frac{1 + 2 \ln(2k_c r/5)}{-\ln^2(2k_c r/5)} \right]^{1/4}. \quad (23)$$

$F_c = E_f S \varepsilon^c$ represents the critical buckling force that the fiber can bear. Eq. (23), which determines the buckling wavelength of a fiber embedded in a soft substrate, is similar to the theoretical solution given by Brangwynne *et al.*¹⁴ For microtubules in living cells, the radius and bending stiffness are taken as 12 nm^1 and $2 \times 10^{-23} \text{ N} \cdot \text{m}^2$, respectively.³⁰ The elastic modulus of the surrounding cytoskeletal network is approximately 1 kPa .^{31, 32} Eq. (23) yields a microtubule wavelength of approximately $2.8 \text{ } \mu\text{m}$, which is similar to the measured value ($\approx 3 \text{ } \mu\text{m}$) by Brangwynne *et al.*¹⁴ and relatively close the value ($\approx 4 \text{ } \mu\text{m}$) in these experiments.

For a fiber with finite length, which is the main concern in this analysis, buckling is expected to occur when the maximum compressive strain in the fiber reaches the critical strain given by eqn (22). Then, from eqns (16) and (22),

$$\varepsilon_0^c = \left[1 + \frac{h-1+h_1}{1+h_1} \frac{4E_f}{G_s c^2} \right] \times \left[\frac{I k_c^2}{S} + \frac{4\pi G_s^*}{-k_c^2 E_f S \ln(2k_c r/5)} \right] \quad (24)$$

When the fiber length is infinite ($1/c = 0$), the critical buckling strain mainly depends on the physical parameters and is independent of the fiber length (eqn (22)). However, if the fiber has finite length, eqn (24) suggests that the critical overall strain ε_0^c in the

substrate depends on the physical parameters of the system as well as the fiber slenderness ratio. The strain in the fiber given by eqn (3) is non-uniform, and eqn (24) is obtained when the maximum compressive strain reaches the critical value given by eqn (22). In this sense, eqn (24) represents an approximate solution. Three-dimensional FE simulations containing more than 40,000 quadratic elements (C3D20R) were conducted to validate the analytical solution given by eqn (24). A perturbation analysis was performed to solve ε_0^c in the simulations with commercial software (ABAQUS). Figure 7 shows that the analytical solution matches the FE results well, indicating that eqn (24) should be useful in practice. The overall critical compressive strain in the substrate, ε_0^c , for the onset of buckling is always greater than that for an infinitely long fiber. The ratio of ε_0^c to ε^c depends on the modular ratio and slenderness ratio of the fiber. $\varepsilon_0^c/\varepsilon^c$ increases when the modular ratio increases or slenderness ratio decreases. Thus, the critical strain ε_0^c in the substrate can be tuned by varying either the slenderness ratio or modular ratio. Eq. (24) is further validated by comparing the critical compressive strains estimated in the experiments with the theoretical predictions shown in Fig. 8. Eq. (24) can indeed provide a reasonable evaluation of the critical buckling strain.

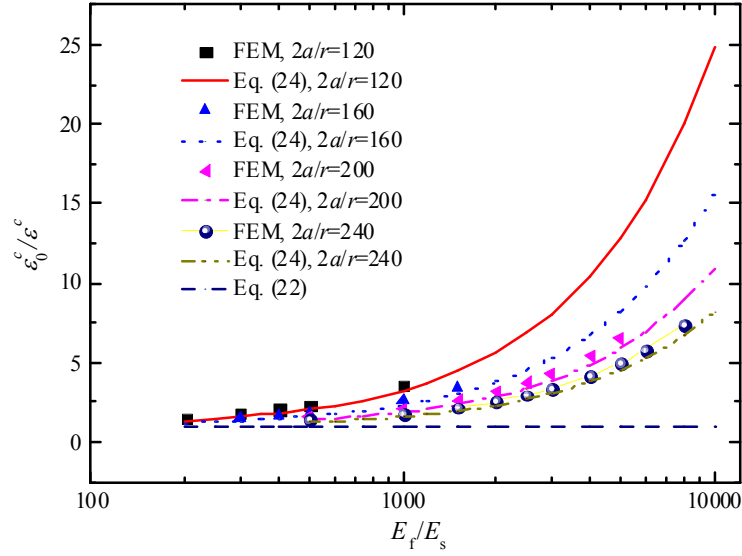


Fig. 7 Ratio of the critical buckling strain ϵ_0^c in the substrate to ϵ^c . The data points refer to the results of FE simulations, and the corresponding lines represent the results predicted with eqns (24) and (22). In the simulation, Poisson's ratios are taken as 0.48 for both the fiber and substrate.

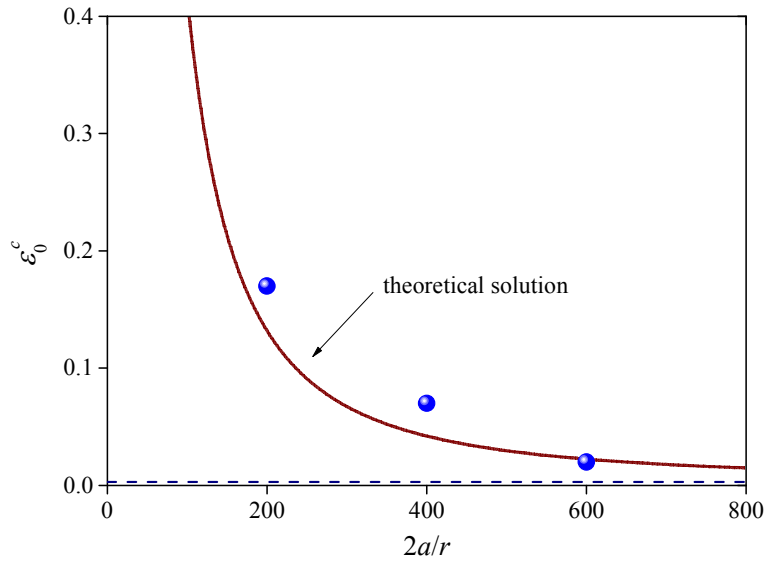


Fig. 8. Effect of the fiber length on the critical strain ϵ_0^c for the onset of buckling. Data points refer to the results estimated from the experiments in Section 2. The solid line represents the theoretical prediction. The dashed line refers to the theoretical solution for a fiber with finite length. In the theoretical solution, Poisson's ratios are both taken as 0.48 for the hair and PDMS substrate.

4. Discussion

Stiff fibers with finite length embedded in a compliant substrate are ubiquitous in both nature and engineering. In these types of systems, compressive forces may not be imposed on the fibers directly. Instead, compression is typically applied on the compliant substrate, and the fibers sense the compression through interfacial shear. For a fiber with infinite length, the strain in the fiber is equal to the overall compressive strain imposed on the substrate. However, for a fiber with finite length, the strain in the fiber can be considerably lower than the overall strain imposed on the substrate and relies largely on the fiber length. The analytical solution obtained in this study suggests that the strain state in the fiber can be quantitatively tuned by controlling either the physical parameters or slenderness ratio of the fiber.

As noted in the theoretical analysis, the interfacial traction is a key factor in the present problem. Recently, Shan *et al.* revealed that the mechanical properties of the fiber-substrate interface played an important role in the attenuated buckling of a biopolymer-reinforced rod.³³ In the current problem, the stress/strain state in the fiber is determined by integrating the interfacial traction directly. Therefore, the interfacial traction directly controls the stress/strain state of the fiber. For an elastic substrate, the interfacial force shown in eqn (1) can accurately describe the interaction between the fiber and substrate, which can be used to evaluate the stress transfer between the fiber and soft matrix in fiber-reinforced composites with low-fiber volume fractions. In biological systems, e.g., microtubules in living cells, the physical properties of the soft matrix typically exhibit spatial variation.³⁴ Thus, the distribution of the interfacial

traction may be dynamically tuned, and then, the stress/strain state and buckling behavior of the fiber can be modulated according to our theory. To further highlight the importance of the interfacial shear, the Appendix provides the derivations for a simple case in which the fiber-substrate interface is weak and the fiber can slide in the substrate. This system may be used to model the fiber-reinforced soil or sand where the interfacial tractions result from friction.³⁵⁻³⁷ Interestingly, the derivations in the Appendix revealed the critical fiber length as

$$\left(\frac{2a}{r}\right)_c = \frac{E_f I k_c^2}{Sf} + \frac{4\pi G_s^*}{-Sf k_c^2 \ln(2k_c r/5)}, \quad (25)$$

beyond which the fiber would buckle into a wavy shape; otherwise, the fiber would maintain a straight configuration and not buckle regardless of the magnitude of the loads imposed on the substrate. Here, f is the friction force at the fiber-substrate interface when sliding occurs.

The key results given by eqns (24) and (25) show that buckling failure may be avoided using the strategy of controlling the slenderness ratio of the fiber and/or modifying the distribution and magnitude of the interfacial shear tractions. These results may help understand some designs in nature, e.g., the dissociative fishbone should have an appropriate slenderness ratio to counteract the buckling caused by the compression due to muscle contractions and guide the development of soft biocomposites where buckling should be prevented or accurately controlled to generate desired patterns across different length scales. Buckling of an elastic fiber embedded in or resting on a soft substrate may also find applications in the mechanical characterization of fibers on small scales.^{14, 19, 38-40} Su *et al.*²³ performed

an interesting study and revealed that a fiber embedded in soft matrix might undergo either planar or non-planar buckling depending on the conditions established in their study. In this sense, when the wrinkling wavelength corresponding to the planar wavy configuration is measured and used to estimate the elastic modulus of the fibers in an inverse analysis, suitable parameters should be selected to avoid non-planar buckling.²³ Moreover, the entropy effect was not considered in this analysis, which might play a role in the cases where the nanofibers are subjected to thermal fluctuations. The entropy effect may be included in the present theoretical model by following the analysis of Hu *et al.*⁴¹ However, this issue is beyond the scope of this study, and further investigation is required.

5. Concluding remarks

The buckling behavior of an elastic fiber with finite length embedded in a soft matrix was investigated through experimental, computational and theoretical efforts. The critical strain imposed on the substrate for the onset of buckling largely depends on the fiber length. The theoretical analysis revealed the important role played by the interfacial traction during the buckling process. An analytical solution was derived to predict the critical condition at the onset of buckling, which was validated with FE simulations. The results may find applications in, for instance, probing the local mechanical environment within cells through the buckling of microtubules, mechanical characterization of micro- or nanowires/fibers, or the design of soft composites.

Acknowledgements

We acknowledge the financial support from the National Natural Science Foundation of China (Grant Nos. 11172155 and 11432008).

Appendix

Here, the effects of interfacial shear tractions on the buckling of a fiber are illustrated by considering the case where the fiber-substrate interface is weak. When the substrate is subjected to compression, the fiber is supposed to slide in the substrate, and interfacial compatibility will not be satisfied. In this case, the interfacial tractions are assumed to be constant:

$$T_z = \begin{cases} -f, & -a < z < 0 \\ f, & 0 < z < a \end{cases} \quad (\text{A1})$$

where f is the friction force at the interface. For a slender fiber, the total friction force acting on the fiber can be considerably greater than the forces at the two ends. In this case, the strain in the fiber under the load $-T_z$ can be obtained as

$$\varepsilon_z^f = -\frac{2}{E_f r} \int_z^a T_z dz = -\frac{2f}{E_f r} (a - z), \quad 0 < z < a \quad (\text{A2})$$

The maximum compressive strain is reached at the center of the fiber, which is given by

$$\varepsilon = -\varepsilon_z^f \Big|_{z=0} = \frac{2fa}{E_f r} \quad (\text{A3})$$

When the maximum compressive strain in the fiber reaches the critical strain given by eqn (22), buckling is supposed to occur. Interestingly, eqns (A3) and (22) give the following critical fiber length:

$$\left(\frac{2a}{r}\right)_c = \frac{E_f I k_c^2}{Sf} + \frac{4\pi G_s^*}{-Sf k_c^2 \ln(2k_c r/5)}, \quad (\text{A4})$$

beyond which the fiber would buckle into a wavy shape; otherwise, the fiber would maintain a straight configuration and not buckle regardless of the magnitude of the loads imposed on the substrate.

References

- 1 B. Alberts, A. Johnson, J. Lewis, M. Raff, K. Roberts and P. Walter, *Molecular Biology of the Cell*, Garland Science, New York, Fourth edition, 2005.
- 2 D. A. Fletcher and R. D. Mullins, *Nature*, 2010, **463**, 485-492.
- 3 J. Howard, *Mechanics of motor proteins and the cytoskeleton*, Sinauer Associates Inc., Sunderland, 2001.
- 4 D. E. Ingber, *Annu. Rev. Physiol.*, 1997, **59**, 575-599.
- 5 N. Wang, J. P. Butler and D. E. Ingber, *Science*, 1993, **260**, 1124-1127.
- 6 N. Wang, K. Naruse, D. Stamenović, J. J. Fredberg, S. M. Mijailovich, I. M. Tolić-Nørrelykke, T. Polte, R. Mannix and D. E. Ingber, *Proc. Natl. Acad. Sci.*, 2001, **98**, 7765-7770.
- 7 W. F. Xue, A. L. Hellewell, W. S. Gosal, S. W. Homans, E. W. Hewitt and S. E. Radford, *J. Biol. Chem.*, 2009, **284**, 34272-34282.
- 8 W. F. Xue, A. L. Hellewell, E. W. Hewitt and S. E. Radford, *Prion*, 2010, **4**, 20-25.
- 9 W. F. Xue, S. W. Homans and S. E. Radford, *Proc. Natl. Acad. Sci.*, 2008, **105**, 8926-8931.
- 10 M. L. Kringelbach, N. Jenkinson, S. L. Owen and T. Z. Aziz, *Nat. Rev. Neurosci.*, 2007, **8**, 623-635.
- 11 J. L. Silverberg, R. D. Noar, M. S. Packer, M. J. Harrison, C. L. Henley, I. Cohen and S. J. Gerbode, *Proc. Natl. Acad. Sci.*, 2012, **109**, 16794-16799.
- 12 G. Whiteley, J. Hewitt and A. Dexter, *Physiol. Plantarum*, 1982, **54**, 333-342.

- 13 P. K. Mallick, *Fiber-reinforced composites: materials, manufacturing, and design*, CRC press, 2007.
- 14 C. P. Brangwynne, F. C. MacKintosh, S. Kumar, N. A. Geisse, J. Talbot, L. Mahadevan, K. K. Parker, D. E. Ingber and D. A. Weitz, *J. Cell Biol.*, 2006, **173**, 733-741.
- 15 M. Dogterom and B. Yurke, *Science*, 1997, **278**, 856-860.
- 16 F. Gittes, E. Meyhöfer, S. Baek and J. Howard, *Biophys. J.*, 1996, **70**, 418.
- 17 G. Brodland and R. Gordon, *J. Biomech. Eng.*, 1990, **112**, 319-321.
- 18 H. Jiang and J. Zhang, *J. Appl. Mech.*, 2008, **75**, 061019.
- 19 T. Li, *J. Biomech.*, 2008, **41**, 1722-1729.
- 20 C. Wang, C. Ru and A. Mioduchowski, *Phys. Rev. E*, 2006, **74**, 052901.
- 21 F. Chiti and C. M. Dobson, *Annu. Rev. Biochem.*, 2006, **75**, 333-366.
- 22 S. G. O'Keeffe, D. E. Moulton, S. L. Waters and A. Goriely, *Int. J. Nonlin. Mech.*, 2013, **56**, 94-104.
- 23 T. Su, J. Liu, D. Terwagne, P. M. Reis and K. Bertoldi, *Soft Matter*, 2014, **10**, 6294-6302.
- 24 H. Cox, *Br. J. Appl. Phys.*, 1952, **3**, 72.
- 25 X. L. Gao and K. Li, *Int. J. Solids Struct.*, 2005, **42**, 1649-1667.
- 26 Z. Wu, J. Ye and J. Cabrera, *J. Mech. Phys. Solids*, 2000, **48**, 1037-1063.
- 27 J. A. Nairn, *Mech. Mater.*, 1997, **26**, 63-80.
- 28 X. Han, Y. Zhao, Y. Cao and C. Lu, *Soft Matter*, 2015, **11**, 4444-4452.
- 29 Y. Zhao, X. Han, G. Y. Li, C. Lu, Y. P. Cao, X. Q. Feng and H. Gao, *J. Mech. Phys.*

- Solids*, 2015, **83**, 129-145.
- 30 F. Gittes, B. Mickey, J. Nettleton and J. Howard, *J. Cell Biol.*, 1993, **120**, 923-934.
- 31 B. Fabry, G. N. Maksym, J. P. Butler, M. Glogauer, D. Navajas and J. J. Fredberg, *Phys. Rev. Lett.*, 2001, **87**, 148102.
- 32 R. Mahaffy, C. Shih, F. MacKintosh and J. Käs, *Phys. Rev. Lett.*, 2000, **85**, 880-883.
- 33 W. Shan, Z. Chen, C. Broedersz, A. Gumaste, W. Soboyejo and C. Brangwynne, *Soft Matter*, 2013, **9**, 194-199.
- 34 M. Jin and C. Ru, *Phys. Rev. E*, 2013, **88**, 012701.
- 35 D. R. Freitag, *J. Geotech. Eng.*, 1986, **112**, 823-826.
- 36 D. H. Gray and H. Ohashi, *J. Geotech. Eng.*, 1983, **109**, 335-353.
- 37 C. S. Tang, B. Shi and L. Z. Zhao, *Geotext. Geomembranes*, 2010, **28**, 54-62.
- 38 Y. P. Cao, X. P. Zheng, B. Li and X. Q. Feng, *Scripta. Mater.*, 2009, **61**, 1044-1047.
- 39 H. Jiang, D. Y. Khang, H. Fei, H. Kim, Y. Huang, J. Xiao and J. A. Rogers, *J. Mech. Phys. Solids.*, 2008, **56**, 2585-2598.
- 40 D. Y. Khang, J. Xiao, C. Kocabas, S. MacLaren, T. Banks, H. Jiang, Y. Y. Huang and J. A. Rogers, *Nano Lett.*, 2008, **8**, 124-130.
- 41 B. Hu, V. Shenoy and Y. Lin, *J. Mech. Phys. Solids*, 2012, **60**, 1941-1951.